Chinese Chemical Letters 34 (2023) 107816

Contents lists available at ScienceDirect

Chinese Chemical Letters

journal homepage: www.elsevier.com/locate/cclet

Density functional theory calculations on 2H-MoS_2 monolayer for HCHO degradation: Piezoelectric-photocatalytic synergy

Yushan Zhu[a], Weina Zhao[a], Binghua Jing[a,b], Junhui Zhou[c], Bihai Cai[a], Didi Li[a], Zhimin Ao[a,c,*]

[a] Guangzhou Key Laboratory Environmental Catalysis and Pollution Control, Guangdong Key Laboratory of Environmental Catalysis and Health Risk Control, School of Environmental Science and Engineering, Institute of Environmental Health and Pollution Control, Guangdong University of Technology, Guangzhou 510006, China
[b] Department of Civil and Environmental Engineering, The Hong Kong University of Science and Technology, Kowloon, Hong Kong 99977, China
[c] Advanced Interdisciplinary Institute of Environment and Ecology, Beijing Normal University, Zhuhai 519087, China

ARTICLE INFO

Article history:
Received 9 March 2022
Revised 30 August 2022
Accepted 8 September 2022
Available online 12 September 2022

Keywords:
Piezoelectricity
Photocatalysis
2H-MoS_2
HCHO
Degradation

ABSTRACT

Formaldehyde (HCHO) is a common indoor gaseous pollutant, and long-term exposure to it may cause serious damage to the human immune system. Photocatalytic degradation of HCHO is a promising technique. However, most photocatalysts have the disadvantage of rapid recombination of photo-generated electron-hole pairs. In this work, the recombination of photogenerated electron holes was proposed to inhibit through the piezoelectric effect. A two-dimensional (2D) piezoelectric material, 2H-MoS_2, was selected to investigate the catalytic performance for HCHO degradation by the synergy of the piezoelectric and photocatalysis properties. The results show that the piezoelectric effect can induce the polarization in 2H-MoS_2 and inhibit the recombination of photogenerated electron-hole pairs, thus improving the photogeneration of hydroxyl radicals for HCHO degradation. Therefore, the piezoelectric-photo-catalysis synergistic effect based on density functional theory (DFT) calculation was proposed to elucidate the HCHO degradation performance. This work could provide important guidance for the development of effective catalysts for HCHO degradation and the application of 2D piezoelectric materials.

Nowadays, with the rapid improvement of the economy and living standards, human society is facing increasing environmental pollution, which has attracted the extensive attention of researchers [1–5]. Formaldehyde (HCHO), as one of the most common indoor air pollutants, normally exists in home, office, building materials, and manufacturing industries, causing serious threat to human health due to the properties of volatility, highly toxicity, and widespreading [6]. Long-term exposure to HCHO causes further injuries for chest, skin, lungs and eyes [6,7]. It is urgent to effectively remove HCHO and avoid secondary pollution [8,9]. On the other side, HCHO is one of the simplest volatile organic compounds (VOCs), which can be used as a model pollutant to explore novel technologies for VOCs treatment.

Photocatalysis is usually adopted for the treatment of HCHO pollutant [10–13]. It possesses low energy consumption, non-toxicity, low cost, and high degradation efficiency with mild reaction conditions [14–18]. The first step in the photocatalytic process is the generation of e-h pairs by photoexcitation. Then these charge carriers immigrate to catalytic activity sites on the surface and participate in redox reactions, producing reactive oxygen species (ROSs), such as hydroxyl radical ($^{\bullet}OH$) and superoxide anion radical ($^{\bullet}O_2^-$) [19,20]. However, most photo-catalysts have the disadvantages of low efficiency of solar energy utilization and rapid recombination of electron-hole pairs [21]. Recently, many experiments improved the degradation performance of VOCs by photoelectric reaction. Huang *et al.* enhanced the photocatalytic activity of CH_3OH-HCHO conversion and the selective oxidation of CH_3OH to HCHO by photoelectric action [22,23]. In 1880, the Curie brothers firstly observed the piezoelectric phenomenon *via* applying mechanical strain to materials [24]. With the external strain, electricity can be generated by internal polarization with positive and negative charges, while it returns a balance state of no charge when without external strain [25,26]. This phenomenon is the piezoelectric effect [27–31]. The generated charges of piezoelectric materials are proportional to the stress applied in catalysts, realizing the conversion between electrical energy and mechanical energy [32]. Piezo-catalysis is a process in which a polarized posi-

* Corresponding author at: Advanced Interdisciplinary Institute of Environment and Ecology, Beijing Normal University, Zhuhai 519087, China.
E-mail address: zhimin.ao@gdut.edu.cn (Z. Ao).

https://doi.org/10.1016/j.cclet.2022.107816
1001-8417/

tive charge is generated at one end and a negative charge is generated at the other end to participate in redox reactions under stress or strain [33,34]. The piezoelectric effect can improve the photocatalytic performance of the catalyst by restraining the recombination of photogenerated electron-hole and improving the ability excitation of light [35–37].

The typical semiconductor of monolayer MoS_2 has emerged enormous potential as piezoelectric photocatalytic material because of the suitable band gap, charged excitons, and valley selective circular dichroism [38]. According to the atomic coordination between the central Mo atom and the surrounding S atom and the stacking sequence of MoS_2 layers, the MoS_2 crystal structure can be divided into four types: 1H, 1T, 2H and 3R, as shown in Fig. S1 (Supporting information) [39]. The 1T MoS_2 has Mo atoms and S atoms coordinate octahedral to form a unit cell; The 1H MoS_2 makes the Mo atoms and S atoms coordinate as octahedron and clamp together in the form of S-Mo-S, which is also the basic unit of MoS_2 monolayer; The 2H MoS_2 has triangular prismatic coordination around Mo atoms, and each element unit has two S-Mo-S units that can be converted from semiconductor to metallic 1T phase by phase engineering; The 3R phase also has the same triangular principal coordination as 2H phase, but with three layers per unit cell along the Z-axis direction [40,41]. The hexagonal polytype layered crystals (2H) are the most common phase, has been widely used as a catalyst for photocatalytic applications [42]. The 1T and 3R phases are metastable, and 2H-MoS_2 is the most stable phase. In addition, monolayer 2H-MoS_2 has a band gap that is more suitable for photocatalytic application [43]. Therefore, 2H-MoS_2 was studied as the catalyst in this paper. As described above, the optical adsorption performance of 2H-MoS_2 is weak due to the limited excitation of visible light and fast electron-holes recombination [44,45]. Strain can be adopted for piezoelectric charges production to promote the separation of electron holes and catalytic activity of catalysts [46–48]. Therefore, the piezoelectric and photocatalytic synergy is considered to solve this particular problem for photocatalysts. In previous studies, the application of MoS_2 for HCHO was mainly used for indoor HCHO detection and sensor applications, but the mechanism process of adsorption and degradation of HCHO by MoS_2 is not clear. Based on this, the mechanism of piezoelectric photocatalytic synergistic degradation of HCHO by MoS_2 is explored in this work [49,50].

2H-MoS_2 is selected as the piezoelectric material to investigate the photocatalytic performance for HCHO degradation in this work. With the effect of strain, the 2H-MoS_2 can generate piezoelectric potential, and forms an internal electric field [51]. The piezoelectric internal electric field can improve the photocatalytic performance of 2H-MoS_2 by inhibiting the recombination of photogenerated electron pairs and promoting the generation of free radicals, which further oxidize HCHO to CO_2 and H_2O. In order to further study the piezoelectric mechanism of 2H-MoS_2 and degradation pathways of HCHO, density functional theory (DFT) calculation can be utilized to better solve those challenges at a microscopic level.

In this work, piezoelectric and photocatalytic synergy was systemically investigated based on DFT calculations on HCHO degradation on 2H-MoS_2. The specific piezoelectric mechanism, photocatalytic activity, and HCHO degradation pathways were confirmed *via* the calculations of the dipole, highest occupied molecular orbital-lowest unoccupied molecular orbital (HOMO-LUMO) distribution, optical absorption spectrum, band structure, deformation density, transition state theory, *etc.* This work not only provides the theoretical guide for the cooperation of piezoelectricity and photocatalysis, but prolongs the application of piezoelectric materials to be photocatalysts.

All calculations were carried out based on spin-unrestricted DFT by Materials Studio. In order to obtain the accurate properties, the CASTEP module was adopted for band structure, work function and optical adsorption spectrum calculations, while the DMol3 module was implemented to calculate absorption and degradation processes for reducing the memory consumption and computing loading [34,52]. The general gradient approximation with Perdew-Burke-Ernzerh function (GGA-PBE) was applied to describe the exchange-correlation interactions [53]. DFT-D correction within the TS scheme was employed to involve the van der Waals correction, expounding the nonbonding interactions [54]. The K-points of $2 \times 2 \times 1$ were used in reciprocal space during the calculations of optical absorption spectrum and electronic structure with a smearing parameter of 5×10^{-3} Ha (1 Hartree = 27.21 eV) [55]. The interactions between the core ions and electrons were employed by utilizing OTFG-ultrasoft pseudopotentials [56–58]. Double numerical plus polarization (DNP) [59] was adopted as the basic set and relativistic effects was sampled by all electron method core treatment. The SCF tolerance, maximum allowed force, displacement and convergence tolerance of energy are 1.0×10^{-6} Ha, 2.0×10^{-3} Ha/Å, 5.0×10^{-3} Å, and 1.0×10^{-5} Ha, respectively. All atoms were allowed to relax in order to obtain more accurate calculation results. The crystal structure of 2H-MoS_2 belongs to the hexagonal structure, the lengths $a = b = 3.15$ Å (are close to the experimental values $a = b = 3.16$ Å), [60] $c = 12.30$ Å and the angles(degrees) $\alpha = \beta = 90°$, $\gamma = 120°$ in lattice constants, which were employed for geometry optimization and the parameters are consistent with those previously reported [61]. Monolayer $4 \times 4 \times 1$ 2H-MoS_2 supercell was constructed with a vacuum level of 30 Å along the Z-axis [62,63].

The adsorption energy (E_{ads}) of HCHO on monolayer 2H-MoS_2 is described by the following equation (Eq. 1):

$$E_{ads} = E_{HCHO+MoS_2} - E_{HCHO} - E_{MoS_2} \quad (1)$$

where $E_{HCHO+MoS_2}$, E_{HCHO} and E_{MoS_2} represent the total energies of HCHO + MoS_2 system, in the same slab, the substrate (MoS_2) and adsorbate system, the isolated substrate (MoS_2) and the free HCHO molecules in the same slab, respectively.

The linear synchronous transit (LST)/quadratic synchronous transit (QST) method with nudged elastic band (NEB) was adopted for transition state theory to search the reasonable pathways of radical generation and HCHO oxidation on monolayer 2H-MoS_2 [59].

The reaction energy (E_{reac}) and energy barrier (E_{bar}) are calculated by the following equations (Eqs. 2 and 3):

$$E_{reac} = E_{FS} - E_{IS} \quad (2)$$

$$E_{bar} = E_{TS} - E_{IS} \quad (3)$$

where E_{FS}, E_{IS} and E_{TS} are the energies of the final, initial, and transition states, respectively. The negative value of E_{reac} represents the exothermic reaction on this system.

Edge positions of the maximum valence band (VBM) and minimum conduction band (CBM) were determined by calculating work function and band gap based on the following equations (Eqs. 4–6) [10]:

$$E_{VBM}\ (eV) = -F + 0.5E_g \quad (4)$$

$$E_{CBM}\ (eV) = -F - 0.5E_g \quad (5)$$

$$E'_{VBM/CBM}\ (V) = -E_{CBM/VBM}\ (pH\ 7) - 4.5 \quad (6)$$

where F and E_g are work function and band gap, $E'_{VBM/CBM}$ is the potential *versus* NHE (pH 7, 0 V *vs.* NHE $\sim$−4.5 eV). The reported chemical potentials to generate free radicals of $^{\bullet}OH$ and $^{\bullet}O^{2-}$ are shown in the following (Eqs. 7 and 8) [64,65]:

$$E^0(O_2/^{\bullet}O_2^-) = 0.13\ V\ vs.\ NHE \quad (7)$$

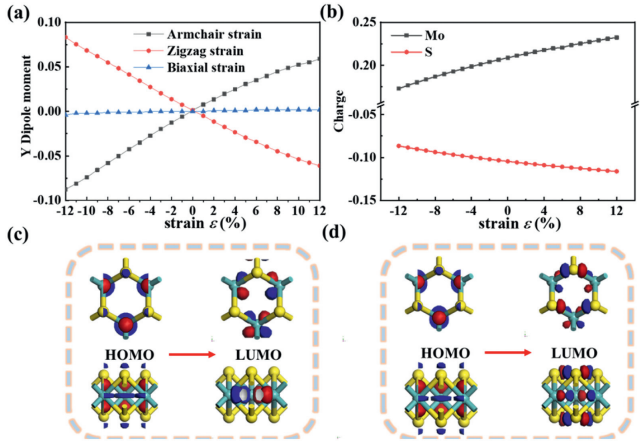

Fig. 1. (a) Y-axis dipole moment of monolayer MoS_2 under uniaxial strains. (b) Hirshfeld charges of single S and Mo atoms in MoS_2 under uniaxial strains of Armchair direction. (c) HOMO-LUMO orbitals of pristine MoS_2. (d) HOMO-LUMO orbitals of MoS_2 with −4% strain along Armchair direction. The yellow and cyan balls respectively represent S and Mo atoms in this and the following figures.

$$E^0(^{\bullet}OH/H_2O) = 2.33\ V\ vs.\ NHE \quad (8)$$

The reaction rate is calculated using the following formula:

$$k = 2.1 \times 10^{10} T e^{-\frac{1000\Delta G^{\neq}}{(1.9859\times T)}} \quad (9)$$

where $\Delta G^{\neq}$, k and T represent the energy barrier, reaction rate and temperature, respectively.

It is concluded from the formula that at room temperature, when the free energy barrier is 21 kcal/mol, it takes only 4.5 min to complete the reaction, and the reaction is relatively fast. Therefore, the energy barrier < 21 kcal/mol is usually used as the standard for single-molecule reactions to determine whether the reaction is prone to occur at room temperature.

In order to explore the piezoelectric-photocatalytic synergy of 2H-MoS_2 to generate ROSs for HCHO degradation, four aspects could be considered in detail: (1) Piezoelectricity of 2H-MoS_2; (2) photocatalysis of 2H-MoS_2; (3) generation of $^{\bullet}OH$ and $^{\bullet}O_2^-$ radicals; (4) pathways of piezoelectric-photocatalytic synergy to degrade HCHO. Subsequently, the mechanism of piezoelectricity-photocatalytic synergy was obtained based on various DFT calculations.

In order to explore the piezoelectricity of 2H-MoS_2 in the system, tensile and compressive strains along with the armchair, zigzag or biaxial direction are imposed to consider all possible situations. It is reported that the effective in-plane strain of MoS_2 monolayer is up to 11%. Thus, the strengths of strain were set from −12% to +12%. Zero represents MoS_2 without strain; "−" and "+" refer to compressive and tensile strains. Dipole moment caused by strains can be used to explore the piezoelectricity due to the positive correlation between internal polarization and piezoelectric strength, while the influence of strains for electronic property can be investigated by charge distribution and frontier orbital. Therefore, dipole moment, charge distribution and orbital including the occupied molecular orbitals (HOMO) and unoccupied molecular orbitals (LUMO) were calculated, and the corresponding results are shown in Fig. 1.

The DFT-derived dipole moments under the strain are shown in Fig. 1a. For biaxial strain, it has little effect for dipole moment, and the situation with biaxial strains will not be further discussed in this work. With the increasing uniaxial strains, dipole moments with compressive strains are higher than that of tensile strains regardless of the armchair or zigzag direction. Moreover, whether the uniaxial strain is along with the armchair or zigzag direction, the direction of the dipole moment remains on the Y-axis. This phenomenon indicates that 2H-MoS_2 polarizes only on the Y-axis. This is consistent with previously reported results [32]. As a result, the piezoelectric effect with compressive strain is stronger than that with tensile strain due to its larger dipole moment under the same strain conditions. Thus, the armchair is acted as the targeted direction to simplify the situation and save computing resources. Furthermore, the in-plane polarization and external current caused by various strains were shown in Fig. S2 (Supporting information). According to the conclusion of dipole moment, polarized charges realized by strains form an internal electric field under the strain and it drives the flow of free charges, producing an electric current. To further understand the relationship between the strain and the direction of the piezoelectric field, the charge distribution of MoS_2 was calculated. Fig. 1b shows the Hirshfeld charges of 2H-MoS_2 with various strains along the armchair direction. Comparing to pristine 2H-MoS_2, the positive charge of a single Mo atom and negative charge of S atom gradually decrease with the enhanced compressive strains, which is opposite with tensile strains. Hence, electrons transfer from Mo to S atoms under tensile strains and S to Mo atoms under compressive strains, producing the internal current and piezoelectric effect. Generally speaking, piezoelectricity is created when it is subjected to a force, the strain that changes the distance between atoms, the variations in the distance between atoms can result in different superpositions of their atomic orbitals [66]. In order to understand the role of strains to internal current and piezoelectricity, HOMO-LUMO orbitals of 2H-MoS_2 with and without strain were calculated. The impact of the piezoelectric effect on 2H-MoS_2 orbitals was studied by taking the pristine and −4% 2H-MoS_2 orbitals as an example, as shown in Figs. 1c and d. The corresponding orbitals with other strains were shown in Fig. S3 (Supporting information). Figs. 1c and d showed that the HOMO orbital of pristine 2H-MoS_2 is mainly distributed on Mo atoms and slightly occupied on S atoms, while LUMO is entirely localized on the Mo atom, indicating the electrons excitation path from S to Mo atoms. However, LUMO of −4% 2H-MoS_2 is mainly covered on S and Mo atoms, triggering the new electrons' migration direction from Mo to S atoms. Fig. S3 showed that when the strain is greater than −4%, the results are similar to those of the strain of −4%, and the tensile strain does not change the electron distribution and direction of 2H-MoS_2. This phenomenon elucidates that the application of compression strains dramatically regulates the electrons' assignment and direction and induces external current, which is advantageous for the piezoelectric effect. Consequently, dipole moment, charge distribution and orbitals of 2H-MoS_2 are regulated by the strains, producing the internal current and piezoelectricity.

Excellent photocatalysts own the properties of reasonable band gap and effective optical adsorption range. A reasonable band gap leads to the feasibility of electron excitation for electron-hole pairs generation. Effective optical absorption range improves the light utilization and photoelectric conversion efficiency [67]. Therefore, band structure and optical absorption spectrum of DFT calculations are important indicators to confirm the photocatalysis of 2H-MoS_2. Fig. S4 (Supporting information) shows the band structure and optical absorption spectrum of 2H-MoS_2 with different strains. As a result, the band gap of monolayer 2H-MoS_2 is 2.28 eV, slightly larger than the experimental value of 1.9 eV [39], which is reasonable and reliable considering the different experimental and theoretical parameter conditions. Fig. S4a shows that the band gap of 2H-MoS_2 increases first and decreases later with the increasing compressive strains, while the tensile strains lead to the decreased band gap in the three systems. Note that depending on the slope of the curve, there are three visible segments. The middle section has the smallest slope, and the remaining two sections have steeper slopes. This indicates that E_g of 2H-MoS_2 is insensitive to low compressive strain. Based on the above results, the piezoelectric effect

of 2H-MoS_2 at low compressive strain is weak, and its band gap increases due to the decrease of lattice parameters. When the compression deformation is large or the tensile strain, 2H-MoS_2 has a strong piezoelectric effect and reduces the band gap by promoting the separation of carriers. Additionally, their tendencies of E_g changes are essentially consistent as a function of strain, which is consistent with results reported in previous studies [68]. As a result, strain can regulate band gap which means piezoelectricity can regulate the photocatalytic properties of 2H-MoS_2.

In order to investigate the effect of strains for optical capacity of 2H-MoS_2, the optical absorption spectrum of 2H-MoS_2 with compressive strains along the armchair direction was considered in Fig. S4b. The corresponding optical adsorption spectrums for other strains were shown in Fig. S5 (Supporting information). Under the compressive strains, a new peak is present in the wavelength range of 200–350 nm and enhances with the increasing strains. This manifests that piezoelectricity induced by strains improves the optical absorption capacity of 2H-MoS_2. Therefore, the piezoelectric effect caused by strains can greatly adjust the band gap and optical absorption capacity of 2H-MoS_2, thereby regulating photocatalysis. Electron density differences of 2H-MoS_2 with strains of −10%, −5%, 0, 5% and 10% in the armchair or zigzag direction were further calculated to understand the effect of piezoelectricity for atomic orbitals, as shown in Fig. S6 (Supporting information). It is observed that the charges are more (less) confined around the atoms under tensile (compressive) strain than under free strain. This indicates that the more ionic component under tensile strain, the more coupling under compressive strain, which is consistent with previously reported results [69]. Consequently, the band gap and optical absorption spectrum of 2H-MoS_2 can be enormously controlled and improved by strains, indicating the significant role of the piezoelectric effect to regulate the photocatalysis of 2H-MoS_2.

$^{\bullet}OH$ and $^{\bullet}O_2^-$ radicals are the dominating ROSs for HCHO degradation on piezoelectric and photocatalytic processes [70]. 2H-MoS_2 with appropriate band edge positions has the potential for $^{\bullet}OH$ and $^{\bullet}O_2^-$ generation, while activation pathways and low E_{bar} confirm the feasibility and accuracy of ROSs production. Thus, the band edge positions of 2H-MoS_2 with different strains, adsorption behavior of H_2O and O_2 on catalysts, and activation pathways and E_{bar} of radicals' generation were analyzed *via* DFT calculations to further confirm the formation of $^{\bullet}OH$ and $^{\bullet}O_2^-$ radicals. The $4 \times 4 \times 1$ supercell of 2H-MoS_2 was applied to release enough sites for H_2O and O_2 adsorption and activation [71].

According to Eqs. 4–6, specific band edge positions of 2H-MoS_2 with various strains were obtained in Fig. S7a (Supporting information). The corresponding work functions (WF), VBM, CBM were shown in Table S1 (Supporting information) and Fig. S8 (Supporting information). The results show that hydroxyl and superoxide radicals can be generated only in the system with a large compression ratio in the armchair direction. Therefore, the −8% and −12% systems are selected for the computational study of HCHO adsorption degradation. As shown in Fig. S7a, the CBM of pristine (0), compressive strain 8% (−8) and 12% (−12) 2H-MoS_2 along armchair direction are 0.129, 0.021 and −0.154 V, respectively, higher than the $O_2/^{\bullet}O_2^-$ redox potential of 0.13 V. The VBM of 0, −8 and −12 2H-MoS_2 are respectively 2.405, 2.749 and 2.355 V, which are over the chemical potential of $^{\bullet}OH/H_2O$ of 2.33 V. This phenomenon indicates that all three systems could generate both $^{\bullet}O_2^-$ and $^{\bullet}OH$, and the efficiency of 2H-MoS_2 with strain is higher than that of pristine 2H-MoS_2. Therefore, both photoelectrochemical processes ($O_2/^{\bullet}O_2^-$ and $^{\bullet}OH/H_2O$) could occur in three systems of 0, −8% and −12% 2H-MoS_2 once the e-h pairs have been photoactivated. Consequently, piezoelectricity caused by strains enhances ROSs production capability, facilitating HCHO degradation on the photocatalysis process.

Band edge positions and oxidation reduction potentials of 2H-MoS_2 imply the capability for ROSs generation, while adsorption behavior of H_2O/O_2 on 2H-MoS_2, and activation pathways of H_2O/O_2 to $^{\bullet}OH/^{\bullet}O_2^-$ can be used to further verify the process. Table S2 (Supporting information) lists the E_{ads} of H_2O and O_2 molecules on 2H-MoS_2 with 0, −8%, −12% strains along the armchair direction. Adsorption energies of H_2O and O_2 under compressive strains have a slight improvement than that on pristine 2H-MoS_2, which creates the conditions of subsequent activation processes.

Transition state theory calculations can be utilized to investigate the activation processes in detail. Specific activation pathways and E_{bar} for $^{\bullet}OH$ generation onto the edges accumulated with piezo-induced h^+ and e^- of 2H-MoS_2 are respectively shown in Figs. S7b-d and Fig. S9 (Supporting information), which show that activation energy barriers on the edges accumulated with piezo-induced h^+ of 2H-MoS_2 under the 0, −8%, and −12% strains are respectively 18.91, 16.84 and 17.07 kcal/mol, indicating the feasibility for hydroxyl groups generation due to the lower E_{bar} than 21 kcal/mol [72]. As shown in Fig. S9, activation energy barriers on the edges accumulated with piezo-induced e^- of 2H-MoS_2 under the 0, −8%, and −12% strains are respectively 29.52, 28.37 and 34.82 kcal/mol, which are above the E_{bar} 21 kcal/mol, indicating the corresponding catalytic systems are difficult to produce hydroxyl groups at room temperature. The results indicate that the piezoelectric effect of the strained 2H-MoS_2 can reduce the energy barrier for water molecules to generate hydroxyl groups, and the corresponding catalytic systems can only produce hydroxyl groups onto edges accumulated with piezo-induced h^+ at room temperature, but not onto the edges accumulated with piezo-induced e^-. This is because h^+ and water react to generate hydroxyl radicals, the edges accumulated with piezo-induced h^+ of 2H-MoS_2 have more h^+ and promote the reaction between h^+ and water, while the edges accumulated with piezo-induced e^- of 2H-MoS_2 inhibit the reaction between h^+ and water. In addition, the electronic spin density of the $^{\bullet}O_2^-$ and −OH moieties was calculated to determine whether the $^{\bullet}O_2^-$ and −OH moieties can exist on the 2H-MoS_2 surface as free radicals, since free radicals usually have characteristic lone-pair electrons, which allows them to be detected by EPR [27]. Figs. S10a and b (Supporting information) describe the structure corresponding to the spin density of systems of $^{\bullet}O_2^-$ and −OH (the formation of hydroxyl groups and S atom on the construction of 2H-MoS_2). It can be seen that the $^{\bullet}O_2^-$ and −OH moieties were $^{\bullet}O_2^-$ and $^{\bullet}OH$, indicating $^{\bullet}O_2^-$ and −OH moieties can exist on the 2H-MoS_2 surface as free radicals. Therefore, the piezoelectric effect can facilitate the production of free radicals on 2H-MoS_2, and it can be determined that free radicals are stable on the surface of 2H-MoS_2, which are used to attack pollutants.

Favorable adsorption behavior between HCHO and 2H-MoS_2 is the precondition to carry out the degradation process. Table S3 (Supporting information) lists various E_{ads} of HCHO on 2H-MoS_2 under compressive strains. The subtle change of E_{ads} suggests the ignorable potency of piezoelectricity for HCHO adsorption.

Based on the adsorption behavior of HCHO on 2H-MoS_2, degradation processes under the 0, −8%, −12% strains were calculated to obtain specific degradation pathways at the microscopic level. $^{\bullet}OH$ radical, as the predominant ROS, was adopted as the model radical for HCHO degradation. According to the first step of the HCHO degradation process, reaction pathways can be divided into two aspects: (1) Hydrogen addition reaction; (2) dehydrogenation reaction and the corresponding structures are shown in Figs. S11a and b (Supporting information).

For the addition reaction shown in Fig. 2, the first step ($HCHO + {}^{\bullet}OH \rightarrow H_2COOH$) is a non-barrier process with the energy release of ∼40 kcal/mol in three catalytic systems (0, −8% and −12% 2H-MoS_2), implying spontaneous process without ex-

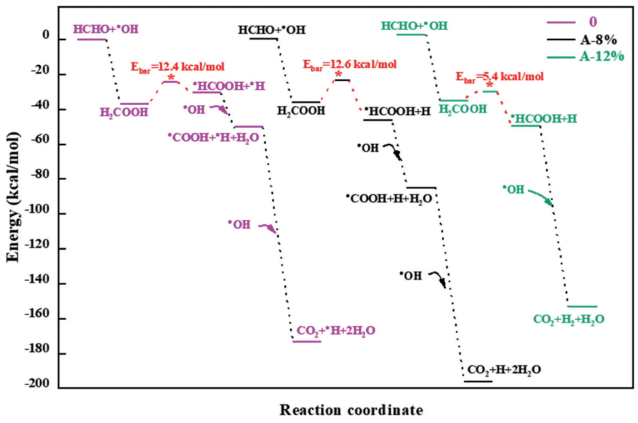

Fig. 2. Degradation pathway including hydrogen addition reaction at the first steps on 2H-MoS_2 with 0, −8% and −12% strains along the armchair direction. Asterisk represents the rate-determining step.

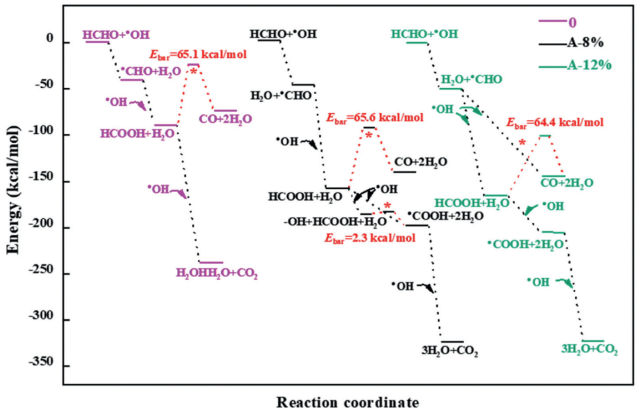

Fig. 3. Degradation pathway including dehydrogenation reaction at the first steps on 0, −8% and −12% 2H-MoS_2 along the armchair direction. Asterisk represents the rate-determining step.

tra energies. Next, the H_2COOH group can be dissociated into one HCOOH group and H atom with low energy barriers in the second step along the three pathways. Particularly in the case of −12% 2H-MoS_2, the low energy barrier of 5.4 kcal/mol and exothermic process with reaction energy of 14.7 kcal/mol manifest the advantage in kinetics and thermodynamics. Subsequently, two $^{\bullet}OH$ gradually take part in the degradation reaction on pristine and −8% 2H-MoS_2 to mineralize HCHO to CO_2 and H_2O. However, one $^{\bullet}OH$ can trigger the mineralization reaction during the catalysis of −12% 2H-MoS_2, indicating the expansionary effect of piezoelectricity for HCHO degradation. Consequently, all the 3 systems can oxidize HCHO into CO_2 and H_2O by $^{\bullet}OH$ radical, while the energy barrier of the rate-limiting step can be enormously regulated and controlled by the strain of 2H-MoS_2, indicating that the significant role of piezoelectric effect on the addition reaction of $^{\bullet}OH$ radical oxidized HCHO.

The degradation pathways with dehydrogenation reaction at the first step were shown in Fig. 3. Similarly, all three systems with 0, −8%, and −12% strains are exothermic processes without energy barriers to take off one H atom for $^{\bullet}CHO$ generation. Subsequently, $^{\bullet}CHO$ reacts with one $^{\bullet}OH$ radical to produce HCOOH in all three systems. Notably, the reaction between $^{\bullet}OH$ and HCOOH cannot carry out due to the participation of H_2O on the pristine 2H-MoS_2 surface. However, the potency of compressive strains for 2H-MoS_2 inhibits the participation of H_2O, thereby mineralizing the HCHO into CO_2 and H_2O. In addition, the reaction steps under −12% strains are simpler than that of −8% strain, suggesting the superior performance of higher compressive strains for HCHO degradation. Considering the toxic by-products, the possibility of CO generation was studied to further explore the degradation process. The energy barriers of 65.14, 65.58 and 64.36 kcal/mol for the three systems are too high to carry out. However, CO can be produced by $^{\bullet}CHO$ and $^{\bullet}OH$ reaction without E_{bar} during the −12% strain. Thus, piezoelectricity triggered by compressive strains boosts the HCHO degradation by $^{\bullet}OH$ radical generated on the photocatalytic process. The strains not only reduce the energy barriers of rate-limiting steps, but also simplify the mineralization process. Additionally, compressive strains limit the participation of H_2O to accelerate the mineralization of HCHO. In general, piezoelectricity has a synergistic effect with photocatalysis for HCHO degradation. The degradation pathways of HCHO by $^{\bullet}O_2^-$ alone and $^{\bullet}OH$ and $^{\bullet}O_2^-$ were also studied. The corresponding structure is shown in Fig. S12 (Supporting information). Fig. S12a shows that the $^{\bullet}O_2^-$ alone does not interact with HCHO, and Fig. S12b shows that when $^{\bullet}OH$ and $^{\bullet}O_2^-$ act on HCHO together, the result is the same as the reaction result of $^{\bullet}OH$ alone. The results show that $^{\bullet}OH$ degrades HCHO and $^{\bullet}O_2^-$ not participate in the degradation of HCHO in the system.

The reaction pathway for HCHO with $^{\bullet}OH$ or $^{\bullet}O_2^-$ radical in the absence of substrate was studied. The results show that there are two different degradation paths of HCHO, one is the reaction of HCHO with 4 $^{\bullet}OH$ radicals to form CO_2 and $3H_2O$ ($HCHO + 4^{\bullet}OH \rightarrow CO_2 + 3H_2O$), the other is the reaction of HCHO with $^{\bullet}OH$ and 2 $^{\bullet}OH$ radicals to form CO_2, H_2O and H_2O_2 ($HCHO + {}^{\bullet}O_2^- + 2^{\bullet}OH \rightarrow CO_2 + H_2O + H_2O_2$) [10]. As mentioned above, compared with the absence of substrate, the pristine 2H-MoS_2 has a higher utilization rate of hydroxyl radical for HCHO degradation, and the 2H-MoS_2 with strain not only improves the utilization rate of hydroxyl radical but also releases more energy.

According to the detailed analysis for piezoelectricity and photocatalysis of 2H-MoS_2, radicals' generation, and HCHO degradation, the mechanism of piezoelectric-photocatalytic synergy for HCHO degradation can be systemically proposed based on DFT calculations. The corresponding mechanism sketch was shown in Fig. S13 (Supporting information).

Under the irradiation of light, electrons of 2H-MoS_2 excite from VB to CB due to the regulation of piezoelectricity for a reasonable band gap. The accumulation of electrons on the CB of 2H-MoS_2 can activate O_2 to generate $^{\bullet}O_2^-$. Meanwhile, the generated holes in the VB would induce H_2O into $^{\bullet}OH$, which further degrades HCHO and mineralizes it into CO_2 and H_2O molecules and $^{\bullet}O_2^-$ does not react with HCHO in this system. Finally, the photogenerated carriers can be effectively transferred and separated by the internal field generated by the piezoelectric effect in the 2H-MoS_2 monolayer, to improve the piezoelectric photocatalytic efficiency of HCHO degradation. In summary, the large compressive strains of 2H-MoS_2 along the armchair generate the built-in electric field, which promotes the effective transfer of photocarriers and inhibits the recombination of photogenerated electron-pairs, thus achieving efficient degradation of HCHO by piezoelectric-photocatalytic synergy in this work. Ultimately, all these results make the 2H-MoS_2 monolayer a potential and effective piezoelectric photocatalyst for VOCs degradation.

The piezoelectricity and photocatalysis of MoS_2 under different strains were systematically studied *via* electronic structure, optical properties, adsorption behavior, radical generation, degradation process, *etc.* Based on the first-principal calculation, the compressive and tensile strains applied to 2H-MoS_2 can not only adjust the band gap and optical absorption capacity, but also generate an internal electric field due to the opposite direction of charge transfer and electron excitation to trigger the piezoelectric effect. In addition, it can reduce the energy barrier of $^{\bullet}OH$ radical generation and promote the degradation process of HCHO to produce

CO_2 and H_2O without the generation of CO byproduct. In addition, the degradation pathways of HCHO were studied in detail. Results shown that the low E_{bar} and high released energies promote the subsequent reaction for HCHO mineralization, and piezoelectricity can further improve the degradation efficiency of HCHO. In general, monolayer 2H-MoS_2 with various piezoelectric strains have excellent photopiezoelectric co-catalytic activity for HCHO, which provides the theoretical guidance for two-dimensional piezoelectric photocatalysts and boosts the practical development in experiment and DFT calculations.

Declaration of competing interest

The authors declare that they have no known competing financial interests or personal relationships that could have appeared to influence the work reported in this paper.

Acknowledgments

This work was financially supported by the National Natural Science Foundation of China (Nos. 22176041 and 41807191), and the Science and Technology Planning Project of Guangdong Province (No. 2017B020216003).

Supplementary materials

Supplementary material associated with this article can be found, in the online version, at doi:10.1016/j.cclet.2022.107816.

References

[1] V. Hasijaa, P. Raizadaa, V.K. Thakurb, et al., J. Environ. Chem. Eng. 8 (2020) 104307.
[2] M.I.A. Abdel Maksoud, A.G. Bedir, M. Bekhit, et al., Environ. Chem. Lett. 19 (2021) 3645–3681.
[3] A. Ishag, Y. Sun, Ind. Eng. Chem. Res. 60 (2021) 8007–8026.
[4] G. Guan, E. Ye, M. You, et al., Small 16 (2020) 1907087.
[5] M. Samadi, N. Sarikhani, M. Zirak, et al., Nanoscale Horiz. 3 (2018) 90–204.
[6] B. Bai, H. Arandiyan, J. Li, Appl. Catal. B: Environ. 142-143 (2013) 677–683.
[7] S. Baroni, S. Gironcoli, A.D. Corso, et al., Rev. Mod. Phys. 73 (2001) 515–562.
[8] S. Lv, Q. Liu, Y. Zhao, et al., J. Phys. Chem. C 123 (2019) 5120–5127.
[9] M. He, J. Ji, B. Liu, et al., Appl. Surf. Sci. 473 (2019) 934–942.
[10] B. Jing, Z. Ao, W. Zhao, et al., J. Mater. Chem. A 8 (2020) 20363–20372.
[11] J. Zhou, G. Liu, Q. Jiang, et al., Chin. J. Catal. 41 (2020) 1633–1644.
[12] W. Liang, J. Li, Y. Jin, Build. Envion. 51 (2012) 345–350.
[13] J. Zhou, D. Li, W. Zhao, et al., ACS Appl. Mater. Interfaces 13 (2021) 23843–23852.
[14] K.K. Gangu, S. Maddila, S.B. Jonnalagadda, Sci. Total Environ. 646 (2019) 1398–1412.
[15] R.V. Solomon, I.S. Lydia, J.P. Merlin, et al., J. Iran. Chem. Soc. 9 (2012) 101–109.
[16] S. Kumar, S. Jain, B.Y. Lamba, et al., Sol. Energy 159 (2018) 423–433.
[17] Z. Zhu, Y. Lin, C. Chung, et al., Appl. Surf. Sci. 543 (2021) 148784.
[18] Y. Liu, X. Hao, H. Hu, et al., Acta Phys. Chim. Sin. 37 (2021) 2008030.
[19] Y. Liu, X. Zeng, X. Hu, et al., Sol. RRL 5 (2020) 2000594.
[20] P. Chen, Y. Zhou, F. Dong, Acta Phys. Chim. Sin. 37 (2021) 2010010.
[21] K. Bisaria, S. Sinha, R. Singh, et al., Chemosphere 284 (2021) 131263.
[22] S. Huang, T. Ouyang, B.F. Zheng, et al., Angew. Chem. Int. Ed. 60 (2021) 9546–9552.
[23] S. Huang, B. Zheng, Z. Tang, et al., Chem. Eng. J. 422 (2021) 130086.
[24] J. Curie, Bull. Soc. Fr. Mineral. 91 (1880) 294–295.
[25] S. Ravinder, M.V. Dahiya, Robotic Tactile Sensing, Springer, Netherlands, 2013.
[26] Z. Liang, C. Yan, S. Rtimi, et al., Appl. Catal. B: Environ. 241 (2019) 256–269.
[27] S. Liu, B. Jing, C. Nie, et al., Environ. Sci. Nano 8 (2021) 784–794.
[28] R. Liu, G. Hu, M. Dan, et al., Nano Energy 72 (2020) 104678.
[29] I. Lee, W. Kang, S. Yong, et al., ACS Nano 13 (2019) 8392–8400.
[30] S. Lan, B. Jing, C. Yu, et al., Small 18 (2022) 2105279.
[31] Q. Liu, W. Zhao, Z. Ao, et al., Chin. Chem. Lett. 33 (2022) 410–414.
[32] M. Dai, W. Zheng, X. Zhang, et al., Nano Lett. 20 (2020) 201–207.
[33] J. Yuan, X. Huang, L. Zhang, et al., Appl. Catal. B: Environ. 278 (2020) 119291.
[34] T. Jia, K. Xu, J. Wu, et al., J. Colloid Interface Sci. 562 (2020) 429–443.
[35] X. Yin, W. Wu, F. Zhang, et al., J. Photochem. Photobiol. A 400 (2020) 112661.
[36] H. Lei, M. Wu, Y. Liu, et al., Chin. Chem. Lett. 32 (2021) 2317–2321.
[37] Y. Chen, X. Deng, J. Wen, et al., Appl. Catal. B: Environ. 258 (2019) 118024.
[38] A. Castellanos-Gomez, H.S.J. van der Zant, G.A. Steele, Nano Res. 7 (2015) 572–578.
[39] Z. Li, X. Meng, Z. Zhang, J. Photochem. Photobiol. C 35 (2018) 39–55.
[40] Z. He, W. Que, Appl. Mater. Today 3 (2016) 23–56.
[41] D. Voiry, A. Mohite, M. Chhowalla, Chem. Soc. Rev. 44 (2015) 2702–2712.
[42] T. Ouyang, J. Guo, H. Shen, et al., Nanoscale 13 (2021) 18192–18200.
[43] R.M. Arif Khalil, F. Hussain, A. Manzoor Rana, et al., Phys. E 106 (2019) 338–345.
[44] E. German, R. Gebauer, Appl. Surf. Sci. 528 (2020) 146591.
[45] K. Paul, N. Sreekanth, R. Biroju, et al., J. Mater. Chem. A 6 (2018) 22681–22696.
[46] R. Roldan, A. Castellanos-Gomez, E. Cappelluti, et al., J. Phys. Condens. Matter 27 (2015) 313201.
[47] E. Scalise, M. Houssa, G. Pourtois, et al., Nano Res. 5 (2011) 43–48.
[48] C. Tan, H. Zhang, Chem. Soc. Rev. 44 (2015) 2713–2731.
[49] G. Choi, R. Mishra, J. Gwag, Mater. Lett. 264 (2020) 127385.
[50] J. Wang, H. Deng, X. Li, et al., Sens. Actuator. B: Chem. 304 (2020) 127317.
[51] W. Wu, X. Yin, B. Dai, et al., Appl. Surf. Sci. 517 (2020) 146119.
[52] T. Ouyang, W. Fan, J. Guo, et al., Phys. Chem. Chem. Phys. 22 (2020) 10305–10313.
[53] Q. Li, L. Xu, K. Luo, et al., Mater. Chem. Phys. 216 (2018) 64–71.
[54] Z. Zhang, Q. Qian, B. Li, et al., ACS Appl. Mater. Interfaces 10 (2018) 17419–17426.
[55] M. Dan, J. Xiang, F. Wu, et al., Appl. Catal. B: Environ. 256 (2019) 117870.
[56] F. Guo, J. Jia, D. Dai, et al., Phys. E 97 (2018) 31–37.
[57] N. Li, Z. Liu, S. Hu, et al., Appl. Surf. Sci. 473 (2019) 70–76.
[58] J.V. Lauritsen, M. Nyberg, J.K. Nørskov, et al., J. Catal. 224 (2004) 94–106.
[59] P. Zheng, A. Duan, K. Chi, et al., Chem. Eng. Sci. 164 (2017) 292–306.
[60] Y. Suo, H. Liu, S. Huang, et al., Appl. Surf. Sci. 437 (2018) 314–320.
[61] M. Kamruzzaman, J.A. Zapien, M. Rahman, et al., J. Alloy. Compd. 863 (2021) 158366.
[62] S. Cheriyan, D. Balamurgan, S. Sriram, Superlattices Microstruct. 116 (2018) 238–243.
[63] Y. Ma, G. Hai, D. Atinafu, et al., J. Colloid Interface Sci. 569 (2020) 89–100.
[64] Z. Cai, X. Hao, X. Sun, et al., Water Res. 162 (2019) 369–382.
[65] Q. Zheng, D.P. Durkin, J.E. Elenewski, et al., Environ. Sci. Technol. 50 (2016) 12938.
[66] D. Szczepanik, J. Mrozek, J. Math. Chem. 51 (2013) 2687–2698.
[67] S. Yu, Q. Li, K. Eshun, ECS Trans. 64 (2014) 25–31.
[68] X. Hu, Q. Zhang, S. Yu, Appl. Surf. Sci. 478 (2019) 857–865.
[69] G.C. Yoon, K.S. Shin, M.K. Gupta, et al., Nano Energy 12 (2015) 547–555.
[70] F. Naumkin, P. del Mazo-Sevillano, A. Aguado, et al., ACS Earth Space Chem. 3 (2019) 1158–1169.
[71] J. Cui, S. Liang, X. Wang, et al., Phys. Chem. Chem. Phys. 17 (2015) 23613.
[72] B. Maryasin, N. Maulide, Eur. J. Org. Chem. 2019 (2018) 338–341.